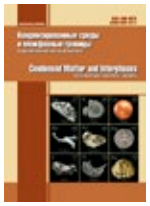

ISSN 1606-867X (Print)
ISSN 2687-0711 (Online)
Condensed Matter and Interphases
Kondensirovannye Sredy i Mezhfaznye Granitsy
https://journals.vsu.ru/kcmf/

Original articles

Research article
https://doi.org/10.17308/kcmf.2023.25/11262

Composition and thermoelectric properties of structures based on iron silicide grown by pulse laser deposition

D. E. Nikolichev✉, R. N. Kriukov, A. V. Nezhdanov, A. V. Zdoroveyshchev, Yu. M. Kuznetsov, V. P. Lesnikov, D. A. Zdoroveyshchev, M. V. Dorokhin, P. B. Demina, A. A. Skrylev

Lobachevsky University,
23 Gagarin av., Nizhny Novgorod 603022, Russian Federation

Abstract

Silicon compounds have a wide range of electrical properties. In particular, the possibility of creating thermoelectric converters based on them looks extremely attractive. The use of most silicides as thermoelectrics today is limited by their low efficiency. The development of approaches consisting in the creation of low-dimensional structures using non-equilibrium formation methods is one of the priority directions for improving the properties of thermoelectric generators. Determination of the effect of technological regimes on the structure, phase-chemical composition and thermoelectric properties of metal-silicide structures is a key task, the solution of which will allow creating highly efficient thermoelectric generators based on them.

Thin-film structures with a layer thickness of ~50 nm formed at different growth temperatures by pulsed laser deposition on two types of substrates: sapphire and gallium arsenide coated with an Al_2O_3 nanolayer were studied in this work. On the formed samples, a chemical analysis and a study of the phase composition were performed. Chemical analysis was carried out by X-ray photoelectron spectroscopy with the chemical composition depth profiling. The phase composition was studied by Raman spectroscopy. In addition, analysis of the elements in the films was carried out by X-ray spectral microanalysis based on a scanning electron microscope. To determine the thermoelectric properties of the formed thin-film structures, the temperature dependences of the Seebeck coefficient and the electrical conductivity coefficient were recorded.

The dependence of the thermoelectric characteristics of iron silicide films on the phase composition is analyzed. In particular, measurements of the thermoelectric properties of $FeSi_x$ thin-film structures registered the manifestation of a strong thermoelectric effect in layers with the maximum number of chemical bonds between iron and silicon. The parameters of the growth process at which the most effective formation of iron-silicon chemical bonds is achieved were determined using the method of X-ray photoelectron spectroscopy. Line shifts from the beta phase of iron disilicide were found in the Raman spectra and the reasons for their appearance were proposed.

Keywords: Iron silicide, Thermoelectric, Pulsed laser deposition, Composition, X-ray photoelectron spectroscopy, Raman spectroscopy

Funding: The work was carried out within the framework of the project N-487-99 under the program of strategic academic leadership «Priority-2030».

For citation: Nikolichev D. E., Kriukov R. N., Nezhdanov A. V., Zdoroveyshchev A. V., Kuznetsov Yu. M., Lesnikov V. P., Zdoroveyshchev D. A., Dorokhin M. V., Demina P. B., Skrylev A. A. Composition and thermoelectric properties of structures based on iron silicide grown by pulse laser deposition. *Condensed Matter and Interphases*. 20223;25(3): 383–391. https://doi.org/10.17308/kcmf.2023.25/11262

Для цитирования: Николичев Д. Е., Крюков Р. Н., Нежданов А. В., Здоровейщев А. В., Кузнецов Ю. М., Лесников В. П., Здоровейщев Д. А., Дорохин М. В., Демина П. Б., Скрылев А. А. Состав и термоэлектрические свойства структур на основе силицида железа, выращенных методом импульсного лазерного осаждения. *Конденсированные среды и межфазные границы*. 2023;25(3): 383–391. https://doi.org/10.17308/kcmf.2023.25/11262

✉ Dmitry E. Nikolichev, e-mail: nikolitchev@phys.unn.ru

1. Introduction

The high potential for the practical application of thermoelectric materials is of considerable interest to scientific groups. Materials based on tellurides and selenides of lead and bismuth today are among the champions in terms of the efficiency of thermoelectric conversion [1-2]. At the same time, there is an active search and development of thermoelectric generators based on silicides of transition *d*-metals (Mn, Fe, Co, etc.) [3]. Interest in thermoelectrics based on silicides is caused, first of all, by the presence of well-established technical processes for creating silicon systems. The variety of phases in metal silicides makes it possible to vary their electronic and photonic properties over a wide range [4-6]. This applies to the same extent to thermoelectric properties.

The dimensionless value of the thermoelectric quality factor $ZT = (\alpha^2\sigma T)/\chi$ determines the efficiency of converting thermal energy into electrical energy at an average absolute temperature T. Due to the high complexity of the experimental determination of thermal conductivity in films, another characteristic is often used that determines the efficiency of a thermoelectric generator: it is the power factor $W = \alpha^2\sigma$ [μW/K^2·m].

The main problem of increasing the efficiency of the thermoelectric parameters of the material is that the thermoelectric quality factor ZT is proportional to the electrical conductivity σ and inversely proportional to the thermal conductivity coefficient χ of the material. Wherein the coefficients σ and χ of the material cannot change independently. An increase in electrical conductivity simultaneously reduces the thermo-EMF coefficient α and leads to an increase in the thermal conductivity of the material.

To reduce the thermal conductivity, the phonon contribution is usually suppressed using defect engineering: 1) the introduction of a high concentration of a substitutional impurity with the creation of a large number of defects due to interstitial atoms [7]; 2) the formation of a nanocrystalline structure with a decrease in thermal conductivity due to the presence of a high concentration of grain boundaries on which phonon vibrations [8] are effectively scattered; 3) the formation of thin films or multilayer structures. In the last two cases the thickness of the crystallite or film becomes an additional degree of freedom in controlling the value of ZT.

In this work, thin films of iron silicides with different Fe content grown at different temperatures are considered. As a method of film formation, we used the method of pulsed laser deposition (PLD) in a vacuum, which has proven itself as a cheap, versatile, and productive method for creating thin-film materials [9]. The study of iron silicides seems promising due to the significant difference in the properties of their phases. Interest in the β-$FeSi_2$ phase in addition to its direct and small band gap [10] arises when this material is used as a thermoelectric energy converter for the range near and below room temperature [11].

At the moment, the maximum ZT for materials based on iron silicides is 0.4 and 0.2 for *n*- and *p*-type semiconductors, respectively. [12]. It is also known that the presence of nanoclusters of this phase formed in epitaxial layers leads to a decrease in the thermal conductivity [13]. The complex of phases of iron silicides (Fe_3Si, FeSi and $FeSi_2$) in the future may have better thermoelectric properties than these phases separately. Structures with thin films, in which the set and content of iron silicide phases are balanced, can potentially act as an efficient thermoelectric converter. Thus, the necessary objective is to determine the phase-chemical composition of thermoelectric systems based on $FeSi_x$.

2. Experimental technique

The structures were formed by pulsed laser deposition in a vacuum chamber with a residual gas pressure of ~ $1\cdot10^{-6}$ Torr.

The composite target was sputtered from the Si and Fe sectors by an LQ-529A pulsed YAG:Nd laser operating at the second harmonic with λ = 0.532 μm. The laser radiation power was ~200 mJ and the pulse duration was 10 ns with a frequency of 10 Hz. The size of the silicon and iron sectors determined the total content of each of the elements in the resulting film. During the first stages, films with a high content of Fe were created, when the angles of the iron sector were ∠ Fe = 240° and ∠ Fe = 120°. Then the angle was reduced to ∠ Fe = 90°. Sputtering was performed

at substrate temperatures of 200, 400, 500, and 550 °C for 40 minutes. The material deposition rate was 1 – 2 nm/min, the average film thickness was ~ 60 nm. The deposition was carried out on two types of substrates: a sapphire (R-cut) and a GaAs (100) substrate with a 20-nm Al_2O_3 layer deposited by vacuum electron evaporation. The choice of substrates is determined by two factors. Firstly, the sapphire substrate does not allow diffusion of material, primarily *d*-metal [14]. Coating the gallium arsenide substrate with a layer of Al_2O_3 also effectively stops this process. [15]. Second, phase states were originally supposed to be recorded by Raman spectroscopy (RS), but the use of a cheap silicon substrate complicates the applying of RS due to the presence of a high-intensity silicon signal from the substrate. As a result, films on a sapphire substrate were used as reference films, while films on a gallium arsenide substrate with an Al_2O_3 layer were used to assess the possibility of forming layers on a semiconductor.

The chemical analysis of the $FeSi_x$/sapphire and $FeSi_x/Al_2O3$/GaAs structures was carried out by X-ray photoelectron spectroscopy (XPS). The spectrometer is part of the Multiprobe RM ultra-high vacuum measuring complex (Omicron Nanotechnology GmbH, Germany). To excite the emission of photoelectrons, Mg K_α radiation was used, and Fe 2*p*, Si 2*s*, Si 2*p*, O 1*s*, C 1*s* photoelectron (PE) lines were recorded. The analysis area diameter was 3 mm. The depth profiling of the composition was carried out by sputtering the layers with Ar^+ ions with an energy of 1 keV at an angle of 45° relative to the sample surface. The numerical values of the concentrations were calculated in accordance with the previously developed method [16].

The chemical shift for the bonding of iron with silicon is not recorded by XPS and this is a serious obstacle in the interpretation of PE lines. The determination of the presence of iron silicide compounds was carried out using the approaches given in [17-18]. To determine the presence of a phase related to iron silicides we used the peaks of photoelectron energy losses on plasmon oscillations, which are recorded for silicides to the left of the main Fe 2*p* doublet at an energy of ~ 730 eV and are absent in the PE spectrum for metallic iron. The intensity ratio of the plasmon loss lines and the main Fe 2*p* doublet is approximately 1:2. This feature made it possible to estimate the concentration of iron in chemical bonding with silicon.

Raman spectra were recorded on an NTEGRA Spectra Raman spectroscopy complex (NT-MDT, Zelenograd) using lasers with a wavelength of 473 nm. The radiation was focused by a 100× objective lens with a numerical aperture of NA = 0.9. The power of unfocused laser radiation measured with a silicon photodetector 11PD100-Si (Standa Ltd, Lithuania) varied in the range from 1 mW to 1 μW. The Raman scattering spectra were recorded in the reflection scheme at room temperature. RS was carried out in the range of 50–900 cm^{-1} with a resolution of 0.7 cm^{-1}.

Electron microscopic imaging, elemental analysis, and element mapping were carried out on a SEM JSM IT-300LV (JEOL, Japan) with an X-MaxN 20 X-ray energy-dispersive spectroscopy set (Oxford Instruments, UK). The measurements were carried out under high vacuum conditions with an electron probe energy of 20 keV. In addition to SEM the surface topography of $FeSi_x$ film was studied using a SolverPro atomic force microscope (NT-MDT, Zelenograd) in semicontact mode.

The temperature dependences of the Seebeck coefficient α and conductivity σ were measured in a Janis CCS-300S/202 closed-loop cryostat with a temperature range of 10–400 K. The sample was pressed with one face to the heater resistor and the other was pressed against a massive heat sink connected to the cooled cryostat rod. To heat up the resistor a Keithley 6221 current source-meter with a current measurement/maintenance accuracy of ~ 2 nA was used. The temperature gradient was stabilized with a LakeShore 335 temperature controller with feedback. The temperature gradient was 10 K with an accuracy of 0.1 K. The thermo-EMF signal was measured using a Keithley 2000 meter [19].

3. Results and discussion

The behaviour of the depth distribution profiles of chemical elements (Fig. 1) demonstrates that, at high Fe concentrations, spatial separation of Si and Fe occurs. It can be seen from Fig. 1a that near the heterointerface the Fe/Si ratio is greater than one and vice versa on the surface.

This circumstance can be explained by the inhomogeneity of the flow of atoms over time during laser deposition. With a decrease in the proportion of metal this inhomogeneity decreases (Fig. 1 b). At the same time a large number of Fe atoms in the layer facilitates the penetration of oxygen atoms into the system (Fig. 1 a). At a lower Fe concentration, the presence of oxygen is not detected. This indicates the concentration dependence of the efficiency of diffusion of oxygen atoms deep into the sample.

It can also be concluded from the behaviour of the Al, O, Si, and Fe profiles at the layer/substrate heterointerface that the Al_2O_3 layer effectively functions as a diffusion barrier. Subsequently, it was determined that the phase distribution is the same for both substrates.

At the same time, the presence of Fe oxide at the film/Al_2O_3 heterointerface (Fig. 1a) indicates the redundancy and physical adsorption of O atoms to Al_2O_3 layers. The composition of the $SiFe_x$ film itself mainly consists of iron silicides which is determined by the distribution profiles of the Fe-Si chemical bond. At the same time, the presence of elemental iron (Fe-Fe bonds) is also recorded and its volume fraction depends on the concentration. At a Fe concentration of 55 at.% only about 30 at.% is spent on the formation of Fe-Si bonds which is about 54 % of the total number of metal atoms. In turn, a decrease in the Fe concentration to 40 at.% leads to the fact that already about 90 % of iron atoms form a chemical bond with Si atoms.

The nonequilibrium process of pulsed laser deposition leads to fluctuations in the distribution profiles of Fe-Fe and Fe-Si chemical bonds. In addition, the applied film formation technology is characterized by the presence of defects on the surface [20]. Drop-like defects are formed due to the presence in the flow of large particles of the substance emitted from the target. Using the method of X-ray spectral analysis performed on the basis of SEM (Fig. 2 a) it was determined that the droplets on the surface consist of both iron and silicon (Fig. 2 b, c). The average size of objects consisting of Si significantly exceeds the diameter of objects consisting of Fe atoms (Fig. 2 b, c) which is caused by different thermodynamic conditions of laser evaporation of the combined Si/Fe target.

Further studies were aimed at studying the phase composition of thin-film structures of iron silicides created by the PLD method with the angle of the iron sector of the sample ∠ Fe = 90° since they demonstrated the almost complete combination of iron with silicon, on the one hand, and still a high concentration of additional phases, providing in the future a decrease in the phonon part of the thermal conductivity, on the other hand. Raman spectra were recorded for $FeSi_x$ films obtained at different temperatures of the Al_2O_3/GaAs substrate (Fig. 3). In all presented Raman spectra one can distinguish peaks related

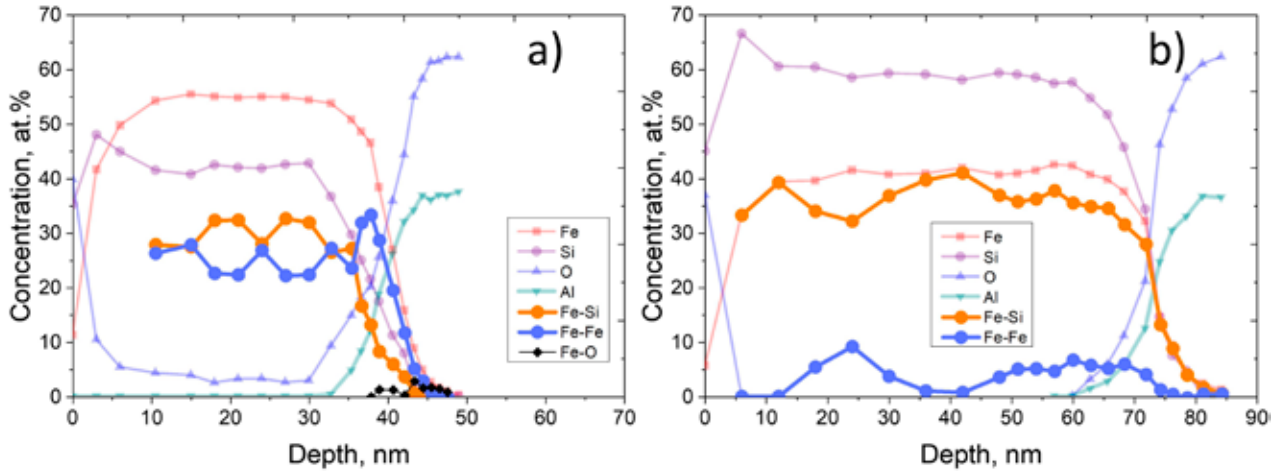

Fig. 1. Depth distribution profile of the concentration of chemical elements and chemical bonds in an $SiFe_x$ film grown on an Al_2O_3/GaAs substrate supersaturated with iron with an iron sector angle of ∠ Fe = 240° (a) and with a reduced iron content with an iron sector angle of ∠ Fe = 90° (b)

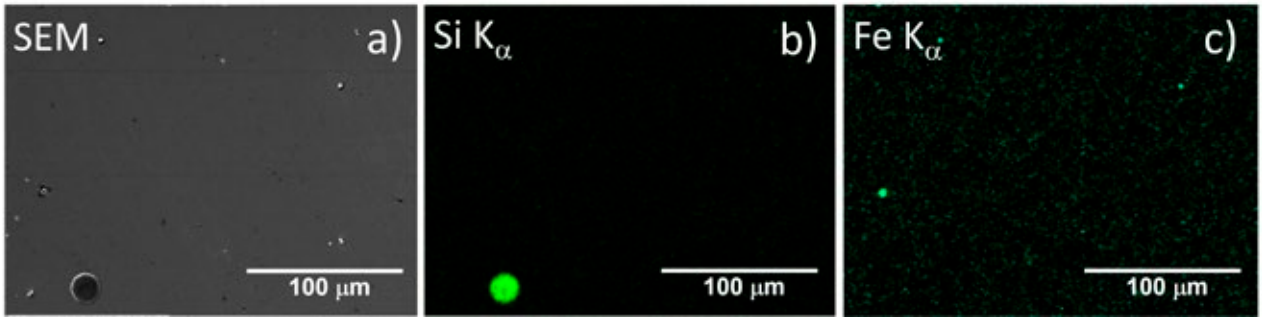

Fig. 2. Topography and elemental composition of the $FeSi_x$ film surface grown at a substrate temperature of 500°C: a) SEM surface image; b) Si distribution map in the Si $K_{\alpha1}$ emission line; and c) Fe distribution map in the Fe $K_{\alpha1}$ emission line

to the GaAs substrate: one of them is located at 268 cm^{-1} and corresponds to the transverse optical component (TO-mode), the second at 291 cm^{-1} belongs to the longitudinal optical component (LO-mode) [21]. Their presence is associated with a small thickness of the film and Al_2O_3 stop layer, as a result of which the signal is detected from the gallium arsenide substrate.

Depending on the substrate temperature during the formation of $FeSi_x$ films, significant changes are observed in the Raman spectra. At a substrate temperature of 200 °C the main contribution to the spectrum is made by a wide continuum related to amorphous silicon in which broad lines can be distinguished in the region of 180 cm^{-1} related to the transverse acoustic mode (TA) and in the region of 480 cm^{-1} related to the transverse optical mode (TO) [22]. The remaining modes from amorphous silicon are weakly expressed, in particular, at 300 cm^{-1} a longitudinal acoustic LA mode is recorded and at 410 cm^{-1} a longitudinal optical LO mode can be found [22]. Also, on the spectrum, there is a weakly pronounced shoulder at 160 cm^{-1} related to the vibrations of the Fe-Fe bonds [23].

Increasing the substrate temperature to 400 °C leads to the appearance of clearly defined lines at frequencies: 193 cm^{-1} with a nearby shoulder at ~ 180 cm^{-1}, ~ 246 cm^{-1} and weakly pronounced broad lines in the regions of 340 cm^{-1} and 385 cm^{-1}. There is also a broad maximum at ~480 cm^{-1} which is related to the transverse optical mode (TO) in amorphous silicon. The presence of lines related to vibrations of Fe-Fe bonds at 193 cm^{-1} and 246 cm^{-1} in the Raman spectrum indicates the formation of a β-$FeSi_2$ crystalline phase in the film [23]. Lines in the regions of 340 cm^{-1} and 385 cm^{-1} may be present, on the one hand, due to the structural imperfection of the film by analogy with the observed peaks in nonstoichiometric $NiSi_2$ [24] and due to second-order scattering, on the other hand [25].

A further increase in the substrate temperature, up to 550 °C leads to a narrowing and an increase in the intensity of the peaks at 193 cm^{-1} and 246 cm^{-1}, as well as to the appearance of a peak at ~ 521 cm^{-1} which belongs to the TO mode of crystalline silicon [26].

It is worth paying attention to the presence of a shift by 2 cm^{-1} in the position of the peak at 246 cm^{-1} related to β-$FeSi_2$. This shift was registered when comparing the spectra of films

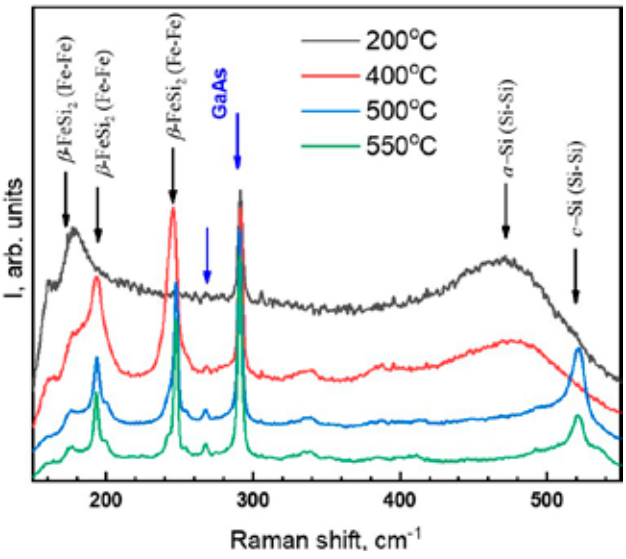

Fig. 3. Raman spectra recorded for $FeSi_x/Al_2O_3/GaAs$ thin-film structures formed at different substrate temperatures in the PLD process

formed at 400 °C and 500 °C. One of the reasons for it can be defects, impurities, lattice distortions of the β-phase of iron disilicide [27]. Another circumstance leading to a shift may be the appearance of a nanocrystalline β-$FeSi_2$ phase by analogy with crystalline silicon [28].

The measurements of Seebeck coefficients, electrical conductivity and calculation of the power factor were carried out for all structures obtained at substrate temperatures of 200, 400, 500, and 550 °C. For all these structures a target with an iron sector ∠ Fe = 90° during the PLD process was used. The characteristic temperature dependences of these parameters are shown in Fig. 4 a–c. Additionally, measurements were made for structures supersaturated with iron in the range of medium temperatures (~ 300–600 °C). The temperature dependence of the power factor for specimens with iron attachment angles on the target ∠ Fe = 120° and ∠ Fe = 240° and a substrate growth temperature of 200 °C is shown in Fig. 4 d.

The electrical conductivity of $FeSi_x$ films at the same *x* depends significantly on the substrate temperature during growth and decreases as it increases. Presumably, this is due to the relaxation of the silicon lattice the formation of iron precipitates and iron silicides [29] in the layer which leads to an increase in the layer resistance. The highest value of the Seebeck coefficient α for samples in which an almost complete combination of iron and silicon has occurred (the angle of iron in the evaporated target ∠ Fe = 90°) is recorded in the low temperature region of about 100 K and its value is ~ 150 μV/K. At lower temperatures α could not be recorded due to a sharp increase in the electrical resistance of the film at temperatures

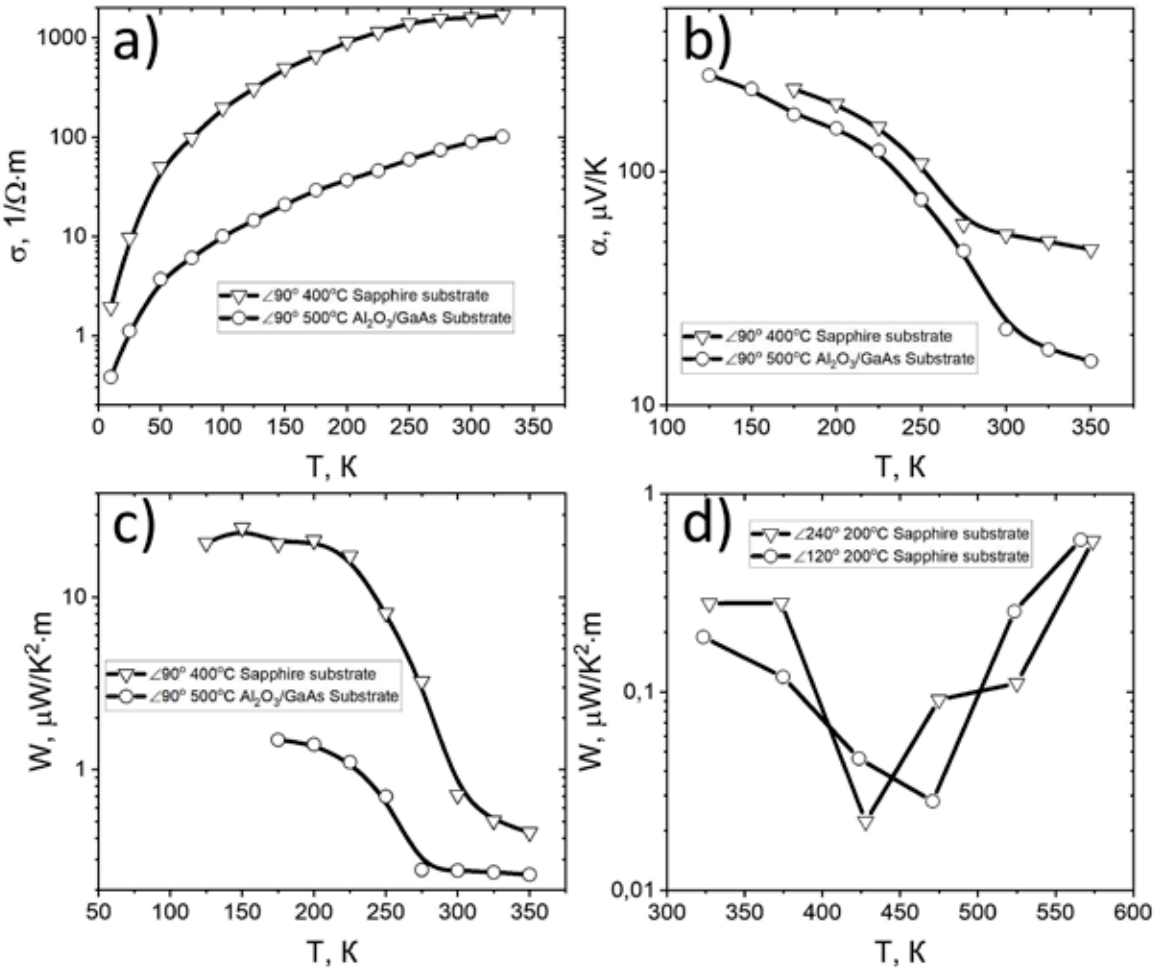

Fig. 4. Temperature dependence of the electrical conductivity coefficient, Seebeck coefficient and power factor for samples with iron sector on a target of ∠ Fe = 90° (a–c) and temperature dependence of the power factor for a Fe-supersaturated film with iron sectors on targets of ∠ Fe = 120° and ∠ Fe = 240° (d)

below 150 K. The maximum calculated value of the power factor *W* (Fig. 4 a) is ~ 20 μW/K²·m. Thus, a sufficiently high value of α is levelled by the low conductivity of thermoelectric films, formed when the iron angle in the evaporated target is ∠ Fe = 90°.

Despite the fact that the electrical conductivity of films supersaturated with iron is 4 orders of magnitude higher at temperatures of 300–600 K, the power factor reaches values only up to tenths of μW/K²·m (Fig. 4 d). This is due to the low efficiency of their thermoelectric conversion, when the maximum value of the Seebeck coefficient does not exceed 10 μV/K. The presence of a minimum in the temperature dependence of the power factor is due to the transition to intrinsic conductivity while the value of the Seebeck coefficient is minimal. Thus, a simple increase in electrical conductivity due to an increase in the iron content does not remove the problem of increasing the power factor, and the solution to this problem lies in the area of optimizing the content of metal-silicide compounds, when the Seebeck coefficient is directly proportional to their amount.

4. Conclusion

The application of X-ray photoelectron spectroscopy and Raman spectroscopy made it possible to find the parameters for the formation of $FeSi_x$ films by pulsed laser deposition, in which iron is almost completely combined with silicon, while the Fe concentration remains at a high level of 40 at.%. XPS depth profiling of the composition of thin-film structures made it possible to determine that an additional Al_2O_3 stop layer formed on a semiconductor substrate by high-vacuum electron evaporation effectively prevents the diffusion-active metal penetrating from the film into the substrate. This is an important technological aspect in the formation of structures under nonequilibrium conditions of the method of pulsed laser deposition and allows the use of a wide range of substrates for the creation of film and multilayer structures with high quality heterointerfaces. Thermoelectric measurements have shown that it is possible to obtain a high thermoelectric effect for films where the iron silicide phase is effectively formed. However, for such structures it is necessary to increase the thermoelectric conversion power factor by increasing the electrical conductivity. This can be facilitated by choosing the growth temperature or parameters of postgrowth annealing of structures that do not lead to the formation of undesirable inclusions in the film material, as well as additional doping of the films with other materials.

Contribution of the authors

The authors contributed equally to this article.

Conflict of interests

The authors declare that they have no known competing financial interests or personal relationships that could have influenced the work reported in this paper.

References

1. Tritt T. M., Subramanian M. A. Thermoelectric materials, phenomena, and applications: a bird's eye view. *MRS Bulletin*. 2006;31: 188–198. https://doi.org/10.1557/mrs2006.44

2. Belonogov E. K., Dybov V. A., Kostyuchenko A. V., Kuschev S. B., Sanin V. N., Serikov D. V., Soldatenko S. A. Modification of the surface of thermoelectric branches based on a Bi_2Te_3-Bi_2Se_3 solid solution by pulse photon treatment method. *Condensed Matter and Interphases*. 2017;19(4): 479–488. https://doi.org/10.17308/kcmf.2017.19/226

3. Rowe D. M. *Thermoelectrics Handbook. Macro to Nano*. New York: CRC Press; 2006. 1008 p. https://doi.org/10.1201/9781420038903

4. Chen L. J. *Silicide Technology for Integrated Circuits*. London: TheInstitution of Engineering and Technology; 2004. 279 p. https://doi.org/10.1049/PBEP005E

5. Wan Q., Wang T. H., Lin C. L. Synthesis and optical properties of semiconducting beta-FeSi2 nanocrystals. *Applied Physics Letters*. 2003;82: 3224–3226. https://doi.org/10.1063/1.1574845

6. Odkhuu D., Yun W. S., Hong S. C. Magnetocrystalline anisotropy energy and spin polarization of Fe3Si in bulk and on Si(001) and Si(111) substrates. *Thin Solid Films*. 2011;519: 8218–8222. https://doi.org/10.1016/j.tsf.2011.03.093

7. Feng X., Fan Y., Nomura N., Kikuchi K., Wang L., Jiang W., Kawasaki A. Graphene promoted oxygen vacancies in perovskite for enhanced thermoelectric properties. *Carbon*. 2017;112: 169–176. https://doi.org/10.1016/j.carbon.2016.11.012

8. Satyala N., Rad A. T., Zamanipour Z., Norouzzadeh P., Krasinski J. S., Tayebi L., Vashaee D. Reduction of thermal conductivity of bulk

nanostructured bismuth telluride composites embedded with silicon nano-inclusions. *Journal of Applied Physics*. 2014;115(4): 044304. https://doi.org/10.1063/1.4861727

9. Zvonkov B. N., Vikhrova O. V., Danilov Yu. A., ... Sapozhnikov M. V. Using laser sputtering to obtain semiconductor nanoheterostructures. *Journal Optical Technology*. 2008;75(6): 389–393. https://doi.org/10.1364/jot.75.000389

10. Liu Z., Osamura M., Ootsuka T., ... Tanoue H. Effect of a Fe_3Si buffer layer for the growth of semiconducting β-$FeSi_2$ thin film on stainless steel substrate. *Journal of Crystal Growth*. 2007;307(1): 82–86. https://doi.org/10.1016/j.jcrysgro.2007.06.007

11. Behr G., Werner J., Weise G., Heinrich A., Burkov A., Gladun C. Preparation and properties of high-purity β-$FeSi_2$ single crystals. *Physica Status Solidi (a)*. 1997;160(2): 549–556. https://doi.org/10.1002/1521-396x(199704)160:2<549::aid-pssa549>3.0.co;2-8

12. Lange H. Electronic properties of semiconducting silicides. *Physica Status Solidi B*. 1997;201(1): 3–65. https://doi.org/10.1002/1521-3951(199705)201:1<3::aid-pssb3>3.0.co;2-w

13. Chen Z.-G., Han G., Yang L., Cheng L., Zou J. Nanostructured thermoelectric materials: Current research and future challenge. *Progress in Natural Science: Materials International*. 2012;22(6): 535–549. https://doi.org/10.1016/j.pnsc.2012.11.011

14. Ohnuma I., Abe S., Shimenouchi S., Omori T., Kainuma R., Ishida K. Experimental and thermodynamic studies of the Fe–Si binary system. *ISIJ International*. 2012;52(4): 540–548. https://doi.org/10.2355/isijinternational.52.540

15. Bobrov A. I., Danilov Yu. A., Dorokhin M. V., ... Syed S. Application of cobalt in spin light Schottky diodes with InGaAs/GaAs quantum wells. *Surface. X-ray, synchrotron and neutron studies*. 2015;7: 57–60. https://doi.org/10.7868/S0207352815070057

16. Boryakov A. V., Surodin S. I., Kryukov R. N., Nikolichev D. E., Zubkov S. Yu. Spectral fit refinement in XPS analysis technique and its practical applications. *Journal of Electron Spectroscopy and Related Phenomena*. 2018;229: 132–140. https://doi.org/10.1016/j.elspec.2017.11.004

17. Ohtsu N., Oku M., Nomura A., Sugawara T., Shishido T., Wagatsuma K. X-ray photoelectron spectroscopic studies on initial oxidation of iron and manganese mono-silicides. *Applied Surface Science*. 2008;254: 3288–3294. https://doi.org/10.1016/j.apsusc.2007.11.005

18. Sidashov A. V., Kozakov A. T., Kolesnikov V. I., Manturov D. S., Yaresko S. I. Surface modification features of tool steels by laser radiation. *Journal of Friction and Wear*. 2020;41(6): 549–553. https://doi.org/10.3103/S1068366620060185

19. Dorokhin M. V., Demina P. B., Erofeeva I. V., ... Trushin V. N. Nanostructured SiGe:Sb solid solutions with improved thermoelectric figure of merit. *Nanosystems: Physics, Chemistry, Mathematics*. 2020;11(6): 680–684. https://doi.org/10.17586/2220-8054-2020-11-6-680-684

20. Demidov E. S., Zubkov S. Yu., Lesnikov V. P., Maksimov G. A., Nikolichev D. E., Podol'skii V. V. X-Ray photoelectron and auger spectroscopy analysis of Ge:Mn-based magnetic semiconductor layers. *Journal of Surface Investigation. X-ray, Synchrotron and Neutron Techniques*. 2008;2(4): 541–545. https://doi.org/10.1134/S1027451008040083

21. Volodin V. A., Sinyukov M. P. Anisotropy of long-wavelength optical phonons in GaAs/AlAs superlattices. *JETP Letters*. 2014;99: 396–399. https://doi.org/10.1134/S0021364014070121

22. Volodin V. A., Koshelev D. I. Quantitative analysis of hydrogen in amorphous silicon using Raman scattering spectroscopy. *Journal of Raman Spectroscopy*. 2013;44: 1760–1764. https://doi.org/10.1002/jrs.4408

23. Terai Y., Yamaguchi H., Tsukamoto H., Murakoso N., Hoshida H. Polarized Raman spectra of β-$FeSi_2$ epitaxial film grown by molecular beam epitaxy. *AIP Advances*. 2018;8: 105028. https://doi.org/10.1063/1.5042801

24. Li F., Lustig N., Klosowski P., Lannin J. S. Disorder-induced Raman scattering in $NiSi_2$. *Physical Review B*. 1990;41(14): 10210–10213. https://doi.org/10.1103/PhysRevB.41.10210

25. Guizzetti G., Marabelli F., Patrini M., Pellegrino P., Pivac B. Measurement and simulation of anisotropy in the infrared and Raman spectra of B single crystals. *Physical Review B*. 1997;55(21): 14290–14297. https://doi.org/10.1103/PhysRevB.55.14290

26. Spizzirri P., Fang J., Rubanov S., Gauja E., Prawer S. Nano-Raman spectroscopy of silicon surfaces. *Materials Forum*. 2008;34: 161–166. https://doi.org/10.48550/arXiv.1002.2692

27. Lefki K., Muret P., Bustarret E., ... Brunel M. Infrared and Raman characterization of beta iron silicide. *Solid State Communications*. 1991;80, 791–795. https://doi.org/10.1103/10.1016/0038-1098(91)90509-T

28. Doğan I., Van De Sanden M. C. M. Direct characterization of nanocrystal size distribution using Raman spectroscopy. *Journal of Applied Physics*. 2013;114: 134310. https://doi.org/10.1063/1.4824178

29. Terukov E. I., Kon'kov O. I., Kudoyarova V. Kh., Gusev O. B., Davydov V. Yu., Mosina G. N. The formation of β-$FeSi_2$ precipitates in microcrystalline Si. *Semiconductors*. 2002;36(11): 1235–1239. https://doi.org/10.1134/1.1521222

Information about the authors

Dmitri E. Nikolichev, Cand. Sci. (Phys.-Math), Associate Professor at the Department of Physics of Semiconductors, Electronics and Nanoelectronics, Lobachevsky University, (Nizhny Novgorod, Russian Federation).
https://orcid.org/0000-0002-0270-850X
nikolitchev@phys.unn.ru

Ruslan N. Kriukov, Cand. Sci. (Phys.-Math), Assistant at the Department of Physics of Semiconductors, Electronics and Nanoelectronics, Lobachevsky University (Nizhny Novgorod, Russian Federation).
https://orcid.org/0000-0001-6684-5899
kriukov@yandex.ru

Alexey V. Nezhdanov, Cand. Sci. (Phys.-Math), Associate Professor at the Department of Physics of Semiconductors, Electronics and Nanoelectronics, Lobachevsky University (Nizhny Novgorod, Russian Federation).
https://orcid.org/0000-0002-7484-106X
nezhdanov@phys.unn.ru

Anton V. Zdoroveyshchev, Cand. Sci. (Phys.-Math), Senior Research Fellow of Laboratory of Spin and Optical Electronics in Physical-Technical Research Institute, Lobachevsky University of (Nizhny Novgorod, Russian Federation).
https://orcid.org/0000-0002-8379-2263
zdorovei@nifti.unn.ru

Yuri M. Kuznetsov, Junior Research Fellow of Laboratory of Spin and Optical Electronics in Physical-Technical Research Institute, Lobachevsky University of Nizhny Novgorod (Nizhny Novgorod, Russian Federation).
https://orcid.org/0000-0001-9450-8953
yurakz94@list.ru

Daniil A. Zdoroveyshchev, Laboratory Technician of Laboratory of Spin and Optical Electronics in Physical-Technical Research Institute, Lobachevsky University of Nizhny Novgorod (Nizhny Novgorod, Russian Federation).
https://orcid.org/0000-0002-2877-4628
daniel.zdorov@nifti.unn.ru

Valery P. Lesnikov, Research Fellow of Laboratory of Spin and Optical Electronics in Physical-Technical Research Institute, Lobachevsky University (Nizhny Novgorod, Russian Federation).
lesnikov@nifti.unn.ru

Michael V. Dorokhin, Dr. Sci. (Phys.-Math), Leading Researcher of Laboratory of Spin and Optical Electronics in Physical-Technical Research Institute, Lobachevsky University (Nizhny Novgorod, Russian Federation).
https://orcid.org/0000-0001-5238-0090
dorokhin@nifti.unn.ru

Polina B. Demina, Junior Research Fellow of Laboratory of Spin and Optical Electronics in Physical-Technical Research Institute, Lobachevsky University (Nizhny Novgorod, Russian Federation).
https://orcid.org/0000-0003-3134-2268
demina@phys.unn.ru

Alexey A. Skrylev, Laboratory Technician of Laboratory of Functional Materials, Lobachevsky University of Nizhny Novgorod (Nizhny Novgorod, Russian Federation).
https://orcid.org/0000-0002-5399-6038
skrylev.lexa@mail.ru

Received 07.12.2022; approved after reviewing 19.12.2022; accepted for publication 26.12.2022; published online 25.09.2023.
Translated by author
Edited and proofread by Valentina Mittova